INSTITUTE OF PHYSICS PUBLISHING JOURNAL OF PHYSICS: CONDENSED MATTER

J. Phys.: Condens. Matter **17** (2005) 6675–6685 doi:10.1088/0953-8984/17/42/008

Radial dependence of the carrier mobility in semiconductor nanowires

Kunal K Das[1] **and Ari Mizel**

Department of Physics, The Pennsylvania State University, University Park, PA 16802, USA

E-mail: kdas@fordham.edu and ari@phys.psu.edu

Received 11 July 2005, in final form 6 September 2005
Published 7 October 2005
Online at stacks.iop.org/JPhysCM/17/6675

Abstract

The mobility of charge carriers in a semiconductor nanowire is explored as a function of increasing radius, assuming low temperatures where impurity scattering dominates. The competition between increased cross-section and the concurrent increase in available scattering channels causes strongly non-monotonic dependence of the mobility on the radius. The *inter*-band scattering causes sharp declines in the mobility at the wire radii at which each new channel becomes available. At intermediate radii with the number of channels unchanged the mobility is seen to maintain an exponential growth even with multiple channels. We also compare the effects of changing the radial scaling of the impurity distribution. We use transverse carrier wavefunctions that are consistent with boundary conditions and demonstrate that the δ-function approximate transverse profile leads to errors in the case of remote impurities.

1. Introduction

The relentless miniaturization of devices has made the physics of lower dimensions a commonplace experimental reality today. A variety of materials are routinely fabricated into nanometre scale elements by research groups around the world; at low temperatures, nanoscale wires can physically behave as one-dimensional conductors in the sense that the carriers are confined to a single, or at most a limited number, of quantum modes or channels in the transverse directions. The study of transport in such one-dimensional conductors continues to reveal novel physical behaviour. In this context semiconducting nanowires in particular have been the focus of sustained study because of the ever-growing technological impact of semiconductors. Several semiconducting materials are being employed to grow nanowires, and to fabricate elementary devices, including silicon [1, 2], gallium arsenide [3, 4], germanium [5, 6], indium phosphide [7, 8] and indium arsenide [9].

[1] Present address: Department of Physics, Fordham University, Bronx, NY 10458, USA.

The carrier mobility is obviously a critical parameter characterizing the transport properties and ultimately the applications potential of a semiconductor nanowire. Experimental studies frequently cite the observed mobility range for samples of interest. For quasi one-dimensional wires made of a specific semiconducting material, the mobility of the carriers depends on several factors, such as the available scattering mechanisms for the carriers, the carrier concentration, the temperature and the physical dimensions of the wire. Numerous theoretical papers [10–18] have studied the influence of essentially every relevant physical parameter on the mobility in ultra-small semiconductor wires. However, such studies have generally been in regimes where either (i) the wires are thick enough and the temperatures sufficiently high that the transport has bulk behaviour, or (ii) they are in the extreme size quantized limit with only one or two channels available. Therefore it is of interest to see how the mobility in a semiconductor nanowire behaves when the number of available channels increases as the wire radius becomes larger and the system deviates from the extreme size quantization limit. That is our goal in this paper. A strong practical motivation exists because with current fabrication methods it is already possible to grow nanowires with specific diameters with a precision of within 10% standard deviation [19–21], and that is certain to improve rapidly with time. We anticipate that careful controlled measurements will be available in the future that will reveal some of the features of the carrier mobility presented in this study.

In some earlier descriptions of mobility in wires at the size quantized regime artificial transverse profiles were sometimes used for the carrier concentration, chosen primarily for mathematical convenience [11, 14]. We treat the carrier transverse motion quantitatively using carrier density profiles that are consistent with physical boundary conditions and considering multiple distinct transverse modes. Size quantization is most pronounced in the regime of very thin wires and low temperatures. Phonon scattering is suppressed at sufficiently low temperatures, so in this paper we work in a regime in which the mobility is mainly determined by impurity scattering. Some recent studies [17] have considered impurities concentrated on the axis. Here, we instead take the impurities to be distributed outside the region of high carrier density since this captures modulation doping [22] or surface roughening effects resulting from some nanowire fabrication methods.

The rest of the paper is arranged as follows. In section 2, we develop the relaxation time description of the mobility applied to one-dimensional systems. We specialize to nanowires with a circular cross-section in section 3 and derive the impurity scattering matrix elements. In section 4, we compute the radial scaling of those matrix elements and of the carrier mobility assuming a surface distribution of impurities. In section 5, we present the results of our numerical calculations and our observations regarding the behaviour of the mobility and related properties as a function of wire radius.

2. Mobility in one dimension in terms of relaxation times

The size quantization limit is most easily achieved at low temperatures when most of the carriers have insufficient energy to populate higher channels. The effect of phonon scattering is negligible at sufficiently low temperatures and impurity scattering is dominant. In order to focus exclusively on the impurity scattering mechanism we consider the degenerate limit corresponding to $T = 0$. Our description will be based on the relaxation time approximation to the Boltzmann equation that approximates the collision term by the quotient of the deviation from equilibrium of the Fermi distribution function and a characteristic relaxation time. In quasi-one dimension, the distribution function $f_i(\mathbf{k})$ carries a continuous label $\mathbf{k}$ for the wavevector along the length of the wire and a set of discrete *channel* indices, denoted by i, that label the degrees of freedom in the restricted transverse dimensions; the same labelling

is used for other physical parameters. Solving the Boltzmann equation in the relaxation time approximation results in a set of equations for the carrier relaxation times τ_i of each channel [23] for a specific energy E:

$$\frac{1}{\tau_i(E)} = \sum_{j,\mathbf{k}'} S_{i,j}(\mathbf{k},\mathbf{k}') \left\{ 1 - \frac{\tau_j(E)}{\tau_i(E)} \cos(\phi) \right\}. \tag{1}$$

Here $S_{i,j}(\mathbf{k},\mathbf{k}')$ is the scattering amplitude from a state in channel i with wavevector $\mathbf{k}$ to another in channel j with wavevector $\mathbf{k}'$. The scattering mechanism satisfies $S_{i,j}(\mathbf{k},\mathbf{k}') = S_{j,i}(\mathbf{k}',\mathbf{k})$. The angle ϕ is between the initial $\mathbf{k}$ and the final $\mathbf{k}'$ wavevectors.

2.1. Scattering matrix in one dimension

In one dimension the wavevectors are scalars, so $\mathbf{k} = \pm k$, allowing only two possible values for the scattering angle, $\phi = 0, \pi$. The total energy of a carrier in the ith channel has two parts:

$$E = \frac{\hbar^2}{2m}(k^2 + \kappa_i^2), \qquad \epsilon_i(k) = \frac{\hbar^2}{2m}k^2. \tag{2}$$

The longitudinal energy $\epsilon_i(k)$ is assumed parabolic with the lattice potential of the semiconductor incorporated into the effective mass m taken to be approximately the same for all channels. The transverse energy $\hbar^2\kappa_i^2/2m$ belongs to a discrete spectrum of energies determined by the boundary conditions of the transverse profile of the wire.

We carry out the sum over final momenta in equation (1) using the Fermi's Golden rule expression for the scattering amplitude:

$$\begin{aligned} \sum_{\mathbf{k}'} S_{i,j}(\mathbf{k},\mathbf{k}') &= \frac{L}{\hbar} \int \mathrm{d}k_j |\langle k', j|V|k, i\rangle|^2 \, \delta\left(\frac{\hbar^2}{2m}(k^2 + \kappa_i^2) - \frac{\hbar^2}{2m}(k'^2 + \kappa_j^2) \right) \\ &= \sum_{\pm} \frac{mL}{\hbar^3 k'} |\langle \pm k', j|V|k, i\rangle|^2. \end{aligned} \tag{3}$$

Energy conservation determines the final wavevector given the initial one and the specific channels involved, $k' = \sqrt{k^2 + (\kappa_i^2 - \kappa_j^2)}$.

2.2. Mobility in one dimension

A knowledge of the scattering matrix determines the relaxation times which in turn determine the electron mobility for each channel in the wire through the expression

$$\mu_i = \frac{q \sum_k v_k^2 [\tau_i(E) \partial_{\epsilon_i(k)} f_i(k)]}{\sum_k f_i(k)} \tag{4}$$

where the carrier velocity for (2) is $v_k = \hbar k/m$. The derivative is with respect to the energy of the free carriers. With E_F denoting the one-dimensional Fermi energy, we can define Fermi energies for *individual* channels $E_i = E_\mathrm{F} - \frac{\hbar^2}{2m}\kappa_i^2$ and the associated Fermi wavevectors. Note that we leave out the label F for Fermi surface quantities for individual channels as superfluous since, as we will see presently, we will only be working with Fermi surface values for each channel. At low temperatures where impurity scattering is most pronounced, the Fermi distribution function is essentially at the degenerate limit:

$$f_i(k) = \theta(E_i - \epsilon_i(k)), \qquad \partial_{\epsilon_i(k)} f_i(k) = -\delta(E_i - \epsilon_i(k)). \tag{5}$$

Allowing for spin degeneracy, the *linear* density of carriers in the ith channel is given by

$$n_{\mathrm{Li}} = 2\int_{-\infty}^{\infty}\frac{\mathrm{d}k}{2\pi}\theta(E_i-\epsilon_i(k)) = \theta(E_i)\frac{2k_i}{\pi}. \tag{6}$$

For a specific carrier density, $n = N/V$, and cross-section A (assumed uniform) of the wire the linear density is $n_{\mathrm{L}} = nA$. Then the one-dimensional Fermi energy E_{F} can be determined by adding together the densities (6) of each channel:

$$\frac{\pi}{2}n_{\mathrm{L}} = \sum_i \theta\left(E_{\mathrm{F}}-\frac{\hbar^2}{2m}\kappa_i^2\right)\sqrt{\frac{2m}{\hbar^2}E_{\mathrm{F}}-\kappa_i^2} \tag{7}$$

where $\theta(x)$ is the Heaviside unit step function. The mobility in each channel becomes

$$\begin{aligned}\mu_i &= -\theta(E_i)\frac{2q\pi}{2k_i}\int_{-\infty}^{\infty}\frac{\mathrm{d}k}{2\pi}\frac{\hbar^2k^2\tau_i(E)}{m^2}\delta\left(E_i-\frac{\hbar^2k^2}{2m}\right)\\ &= -\theta(E_i)\frac{q\tau_i(E_{\mathrm{F}})}{m}.\end{aligned} \tag{8}$$

The average mobility for electrons is then given by

$$\mu = \frac{\sum_i n_{\mathrm{Li}}\mu_i}{\sum_i n_{\mathrm{Li}}} = \theta(E_i)\frac{e}{m}\frac{\sum_i k_i\tau_i(E_{\mathrm{F}})}{\sum_i k_i}. \tag{9}$$

In the degenerate limit the relaxation times have to be evaluated *only* at the Fermi surface determined by the total carrier density in the wire and the wire radius.

3. Cylindrical nanowires

We will now specifically consider nanowires with an uniform cylindrical cross-section, and a Coulomb scattering potential arising from ionized impurities. At low temperatures where impurity scattering is dominant a Coulomb potential is an appropriate choice for the scattering potential V in typical low-dimensional systems. The natural basis consists of a product of transverse functions involving Bessel functions and a plane wave corresponding to the longitudinal part. The matrix element due to an impurity at $\mathbf{r_0} \equiv \{z_0, r_0, \theta_0\}$ is

$$\begin{aligned}\langle k_j, j|V(\mathbf{r},\mathbf{r_0})|k_i, i\rangle = \frac{e^2}{4\pi\epsilon L}\int_0^R r\,\mathrm{d}r\int_0^{2\pi}\mathrm{d}\theta\,\Phi_j^*(r,\theta)\Phi_i(r,\theta)\\ \times\int_{-\infty}^{\infty}\mathrm{d}z\frac{\mathrm{e}^{-\mathrm{i}(k_j-k_i)z}}{\sqrt{(r^2+r_0^2-2rr_0\cos(\theta))+(z-z_0)^2}}\end{aligned} \tag{10}$$

where the azimuthal angle θ is measured from the direction of the impurity at θ_0. Because of the cylindrical symmetry the value of θ_0 will not influence the scattering probability. The quantity ϵ is the dielectric constant. It is well known [12] that due to screening of the Coulomb interaction, in the strict degenerate limit of zero temperature the static dielectric function in one dimension evaluated in a random phase approximation (RPA) has a divergence at twice the Fermi vector, $2k_i$, for a channel. From our analysis above it is clear that for intra-channel scattering at the degenerate limit the momentum change corresponds precisely to that value, and therefore the dielectric constant also needs to be evaluated at that divergent point. However, our interest is in the radial scaling of the mobility and not on evaluating its precise value, so we adopt the assumption of low, but *non-zero*, temperature used in a similar context in [14], whereby the divergence is removed leading to a well-defined dielectric function. The analysis of [14] also showed that a doubling of the wire radius caused relatively small changes in the

dielectric constant over a wide range of carrier densities. But as we will establish in this paper, the effects of increasing radius on the mobility on the other hand is exponential in nature. Therefore the dependence of the dielectric function on wire size should have little qualitative impact on the radial scaling of the mobility. Hence we will treat the dielectric function as a constant ϵ over the range of radii that we consider in this paper.

The transverse wavefunctions involve Bessel functions and for a wire of radius R are given by

$$\Phi_i(r,\theta) = \frac{\mathrm{e}^{\mathrm{i}l\theta}}{\sqrt{2\pi}} \frac{J_l(\kappa_{ln} r)}{\frac{R}{\sqrt{2}} J_l'(\kappa_{ln} R)}. \tag{11}$$

The various channels are labelled by two indices $i \equiv l, n$, with l corresponding to the order of the Bessel functions $J_l(\kappa_{ln} r)$, and n labelling the zeros for each order in a sequence of increasing magnitude. The transverse eigenmodes are determined by the boundary condition that the Bessel functions vanish on the surface of the wire $J_l(\kappa_{ln} R) = 0$, with the zeros denoted by $p_{ln} = \kappa_{ln} R$.

We assume a azimuthally symmetric layer of impurities of bulk density $\rho(r_0)$ distributed between radii $r = a$ and $r = b$. On integrating over the impurity distribution we obtain the scattering amplitude sum (3):

$$\begin{aligned}\sum_{\mathbf{k}'} S_{j,i}(\mathbf{k}', \mathbf{k}) &= L \int_a^b \mathrm{d}r_0\, 2\pi r_0 \rho(r_0) \sum_{\pm} \frac{mL}{\hbar^3 k'} |\langle \pm k_{l'n'}, l'n' | V(\mathbf{r}, \mathbf{r}_0) | k_{ln}, \ln \rangle|^2 \\ &= S^{+}_{l'n',ln} + S^{-}_{l'n',ln}\end{aligned} \tag{12}$$

with

$$\begin{aligned}S^{\pm}_{l'n',ln} = \frac{me^4}{2\pi\epsilon^2\hbar^3} \times \frac{1}{k_{l'n'}} \int_a^b \mathrm{d}r_0\, r_0 \rho(r_0) \Bigg| \int_0^R r\mathrm{d}r \int_0^{2\pi} \frac{\mathrm{d}\theta}{2\pi} \frac{J_{l'}(\kappa_{l'n'} r) J_l(\kappa_{ln} r) \mathrm{e}^{\mathrm{i}(l'-l)\theta}}{\frac{R^2}{2} J_{l'}'(\kappa_{l'n'} R) J_l'(\kappa_{ln} R)} \\ \times K_0\left(|k_{ln} \mp k_{l'n'}| \sqrt{r^2 + r_0^2 - 2rr_0\cos(\theta)} \right) \Bigg|^2.\end{aligned}$$

The + sign corresponds to forward scattering ($\phi = 0$) and the − to backscattering ($\phi = \pi$). Using this notation in equation (1) gives a system of linear equations for the relaxation times:

$$\left[2S^{-}_{ln,ln} + \sum_{\{l'n'\} \neq \{ln\}} \left(S^{+}_{l'n',ln} + S^{-}_{l'n',ln} \right) \right] \tau_{ln} + \sum_{\{l'n'\} \neq \{ln\}} \left(S^{-}_{l'n',ln} - S^{+}_{l'n',ln} \right) \tau_{l'n'} = 1. \tag{13}$$

At zero temperature the matrix elements, like the relaxation times, are evaluated at the effective Fermi wavevector k_{ln} for each channel. In the strict one-dimensional limit when only the lowest channel is available we retrieve the well-known result $\tau^{-1} = 2S^{-}_{01,01}$ [11]. It has been a common practice to assume that in thin wires the carriers may be assumed to be confined to the wire axis, thereby justifying the usage of a δ-function to approximate the transverse profile of the carrier density, in which case the matrix elements in equation (12) reduce to

$$S^{\pm}_{l'n',ln} \simeq \frac{me^4}{2\pi\epsilon^2\hbar^3 k_{l'n'}} \int_a^b \mathrm{d}r_0\, r_0 \rho(r_0) K_0^2[|k_{ln} \mp k_{l'n'}| r_0]. \tag{14}$$

While this is mathematically simpler, we will presently show that this approximation is invalid for the cases we consider.

4. Surface impurities

For some quasi-one dimensional nanowires, it is a good approximation to treat the impurities as distributed in a layer of varying thickness outside the wire; this models surface roughness

or modulation doping of dopants. We therefore take the scattering centres to be distributed in a thin uniform layer of width w along the surface of the wire. First we take the bulk density of the impurities to be constant within that layer $\rho(r_0) = \rho_B$. We then write the matrix elements in equation (12) in a way that makes the radial dependence more transparent:

$$S^{\pm}_{l'n',ln} = Q \times \frac{(R/l_0)^2}{q_{l'n'}} \left| \int_0^1 x\,\mathrm{d}x \frac{J_{l'}(p_{l'n'}x)J_l(p_{ln}x)}{\frac{1}{2}J'_{l'}(p_{l'n'})J'_l(p_{ln})} \right.$$
$$\left. \times \int_0^{2\pi} \frac{\mathrm{d}\theta}{2\pi} \mathrm{e}^{\mathrm{i}(l'-l)\theta} K_0\left(|q_{l'n'} \mp q_{ln}|\sqrt{1+x^2-2x\cos\theta}\right) \right|^2. \tag{15}$$

Everything that does *not* depend on the radius has been included in the pre-factor Q which contains all the dimensioned quantities. The rest of the expression contains only *dimensionless* quantities as we have rescaled the lengths by the radius R, so that the integration variable is $x = r/R$ and the wavevectors are $q = Rk$. The scale and the dimension of the matrix element are then set by the constant in front:

$$Q = \frac{me^4 l_0^3 n}{2\pi\epsilon_0^2\hbar^3} \times \left[\frac{1}{\epsilon_s^2}\frac{m}{m_e}\frac{\rho_B}{n}\frac{w}{l_0}\right] = 1.04 \times 10^{15}\ \mathrm{s}^{-1} \times \left[\frac{1}{\epsilon_s^2}\frac{m}{m_e}\frac{\rho_B}{n}\frac{w}{l_0}\right]. \tag{16}$$

We have assumed a length scale of a nanometre $l_0 = 10^{-9}$ m along the radial direction, for the wire radius R as well as for the width of the scattering layer w. We have also scaled the impurity density ρ_B by the carrier density n. The dielectric constant of the wire is denoted by ϵ_s.

Another advantage of writing the matrix elements this way lies in the fact that the factor Q is common to all the matrix elements $S^{\pm}_{l'n',ln}$ in the set of linear equations in equation (13). We can therefore divide through by that factor, and since the multiplication of a column of a determinant by a constant has the effect of multiplying the determinant by the same constant, all the relaxation times τ_{ln} for every channel carry a common factor of Q^{-1}.

In certain cases it is more accurate to assume that the linear density of the impurities is constant instead of the bulk density of impurities. In that case the radial scaling is somewhat different; we then have to replace $w\rho_B \to \rho_L/(2\pi R)$ so that the scattering matrix elements are

$$S'^{\pm}_{l'n',ln} = Q' \times \frac{(R/l_0)}{q'} \left| \int_0^1 x\,\mathrm{d}x\, \frac{J_{l'}(p_{l'n'}x)J_l(p_{ln}x)}{\frac{1}{2}J'_{l'}(p_{l'n'})J'_l(p_{ln})} \right.$$
$$\left. \times \int_0^{2\pi} \frac{\mathrm{d}\theta}{2\pi} \mathrm{e}^{\mathrm{i}(l'-l)\theta} K_0\left(|q_{l'n'} \mp q_{ln}|\sqrt{1+x^2-2x\cos\theta}\right) \right|^2. \tag{17}$$

The coefficient Q' has the same scale factor as Q, but now the bulk impurity density and the width of the impurity layer are replaced by a linear density of the impurities ρ_L, scaled by the bulk carrier density and a nanoscale area element $n \times 2\pi l_0^2$:

$$Q' = \frac{me^4 l_0^3 n}{2\pi\epsilon_0^2\hbar^3} \times \left[\frac{1}{\epsilon_s^2}\frac{m}{m_e}\frac{\rho_L}{2\pi l_0^2 n}\right]. \tag{18}$$

5. Results and discussion

We now proceed with numerical estimates for gallium arsenide (GaAs) for which our assumption of parabolicity (2) is appropriate. Since we are interested mainly in the radial scaling we present our results scaled by the common constant Q since it carries no radial dependency. But it determines the intrinsic magnitude of the physical quantities; therefore,

Table 1. The zeros p_{ln} of the Bessel functions, for the lowest transverse channels in a uniform cylindrical wire, are listed along with the minimal values of the scaled wire radius $n^{1/3}R$ at which each channel becomes populated with charge carriers. For a bulk carrier density of $n = 10^{24}$ m^{-3} that we use for numerical estimates, the right column would correspond to radii in units of 10^{-8} m $= 10$ nm.

p_{ln}	$n^{1/3}R$
$p_{0,1} = 2.404\,82$	0
$p_{1,1} = 3.831\,71$	0.8455
$p_{2,1} = 5.135\,62$	1.173
$p_{0,2} = 5.520\,07$	1.305
$p_{3,1} = 6.380\,16$	1.539
$p_{1,2} = 7.015\,59$	1.706
$p_{4,1} = 7.588\,34$	1.856
$p_{2,2} = 8.417\,24$	2.048
$p_{0,3} = 8.653\,72$	2.116

we first provide an estimate of its value for a GaAs nanowire. The effective mass for GaAs is $m = 0.068m_e$, assumed the same for all the channels, and the dielectric constant is about $\epsilon_s = 12$, not significantly altered by screening at the high carrier density that we consider [14]. If we take the impurity density to be equal to the carrier density and the impurity layer to be of the order of a nanometre thick $w \simeq 10^{-9}$ m, we obtain a value of $Q \simeq 4.9 \times 10^{11}$ s^{-1}. We may then estimate the magnitude of the average mobility by writing it as

$$\mu = \frac{e}{Qm}\theta(E_i)\frac{\sum_i q_i[Q\tau_i(q_i)]}{\sum_i q_i}. \tag{19}$$

The pre-factor contains all the dimensioned quantities and, for the above-mentioned value of Q, it is $e/(Qm) \sim 5 \times 10^4$ cm^2 V^{-1} s^{-1}. Our numerical computation of the remaining dimensionless part, presented below, then yields a mobility in the range $10^4 - 10^7$ cm^2 V^{-1} s^{-1}, which is consistent with the magnitudes in experimental measurements.

Having established the range of magnitudes of the mobility we now turn our attention to the radial scaling. The numerical estimates assume a carrier density of 10^{18} cm^{-3} $= 10^{24}$ m^{-3}. When all else is fixed the radius determines the number of channels available for transport in equation (7). The minimal radii for each channel to be populated with carriers having non-vanishing longitudinal energy are shown in table 1.

In figure 1(a) we plot the modified Bessel function of the second kind for the lowest channel, $K_0(x, \theta; q_{01}) = K_0(2q_{01}\sqrt{1 + x^2 - 2x\cos(\theta)})$; it contains the effects of the Coulomb scattering in the scattering matrix elements. In the x–θ plane, the function $K_0(x, \theta; q_{01})$ is very strongly peaked along the $\theta = 0$ line; therefore, we specifically chose to plot $K_0(x, 0; q_{01})$. In order to see the behaviour over the entire range of wire radii we present plots for the minimum radius $R = 5$ nm and maximum radius $R = 18.5$ nm that we consider. Alongside we plot the unnormalized radial profile of the carrier density in the lowest channel $J_{01}(p_{01}x)$. We find that the *overlap* of the carrier density profile $J_{01}(p_{01}x)$ with the prominent region of $K_0(x, \theta; q_{01})$ decreases significantly with increased wire radius, indicating that an approximation that replaces the radial profile with a delta function at the wire axis would deteriorate rapidly with larger wire radius. That is exactly what we see in figure 1(b) where we plot the intra-band scattering matrix element $S^-_{01,01}$ for the lowest channel using first equation (12) which uses the appropriate radial profile and secondly equation (14) which uses the δ-function approximation. The two curves are noticeably different even for a wire radius of 5 nm, but for larger wire radii they differ by several orders of magnitudes. This is exactly what one would expect for a surface

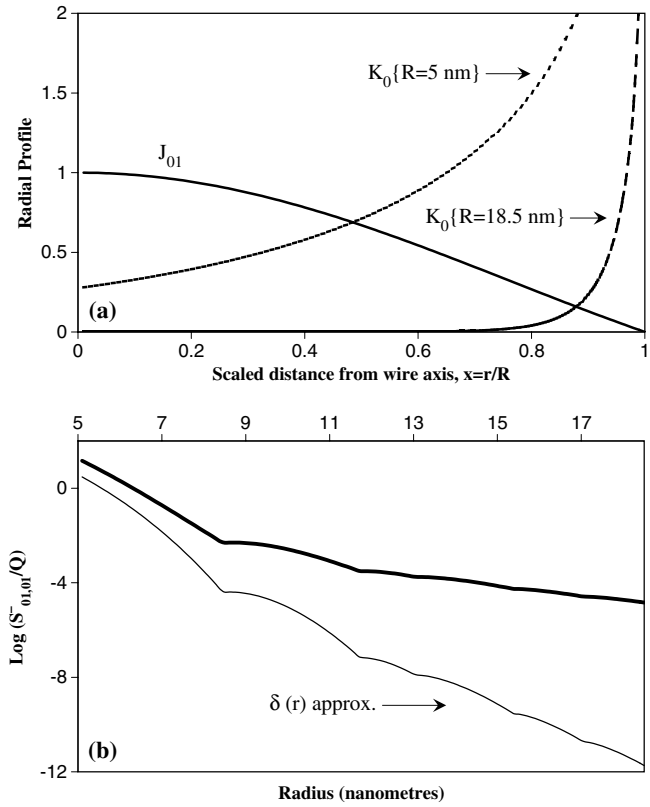

Figure 1. (a) Plot of the radial profile of the carrier distribution of the lowest channel, $J_{01}(p_{01}x)$, shown alongside the radial dependence of the impurity scattering contained in the factors $K_0(2q_{01}|1-x|)$ shown for the extreme values of the range of wire radii R that we consider. (b) Semi-log plot of the scattering matrix element, scaled by the constant Q, for the lowest channel with (thin line) and without (thick line) the δ-function approximation for the radial density of the carriers.

distribution of impurities because the impurities are further removed from the wire axis for a larger wire.

Figure 2 shows the scaling of the Fermi wavevector with the radius. We see that the dimensionless product of the wire radius with the Fermi wavevector, $R \times k_F$, has an almost monotonic growth with the radius. The Fermi vector itself decreases noticeably as each new channel becomes available, and then rebounds gradually but with an overall decline of the peak values reached before each succeeding channel enters. So the general trend is that k_F gets smaller with increasing radius; with a sufficiently large number of channels we expect it to approach the bulk value which, for the carrier density we have assumed, would be $k_F^{3D} = (3\pi^2 10^{-24})^{1/3} \sim 0.31\ \mathrm{nm}^{-1}$. Our plot suggests a gradual approach to that limit. That limit gives a criterion for when the system makes the transition from quasi-1D to 3D.

We plot the mobility in figure 3 on a logarithmic scale to show that the growth of the mobility with radius is of an exponential nature in between points of sharp declines. The most striking feature is that the multichannel scattering destroys the simple monotonic growth of the mobility seen with a single channel [11]. As the radius increases, and each new channel becomes energetically available for scattering there is a sharp reduction in the average mobility.

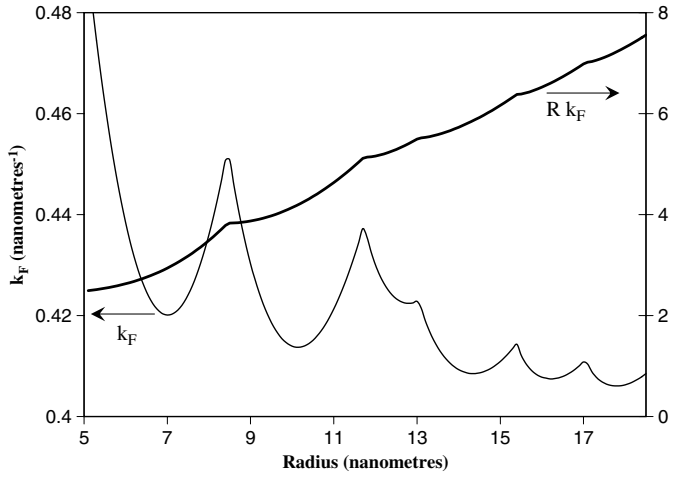

Figure 2. The net Fermi wavevector $k_F = \sqrt{2mE_F/\hbar^2}$, for the carriers in the wire for a fixed carrier density $n = 10^{24}$ m^{-3}, is plotted along the left axis as a function of the radius. The dimensionless quantity Rk_F is plotted along the right axis.

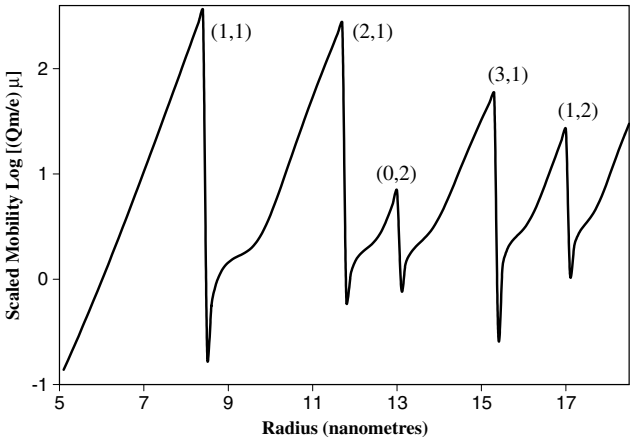

Figure 3. The mobility scaled by $e/(Qm)$ is plotted on a logarithmic scale as a function of the wire radius for fixed carrier $n = 10^{24}$ m^{-3}. The (l, n) label for each new channel is shown as it becomes available causing the sharp declines in the mobility.

In between the addition of new scattering channels, the increasing wire radius causes the mobility to grow, but that growth has an inflection point, reflecting the competition of that tendency with increased inter-channel scattering. The sharp declines cause an overall lowering of the mobility as the radius increases significantly. This is consistent with an eventual approach to bulk behaviour.

We get a sense of the actual intrinsic magnitude of the mobility and its variations in figure 4 where a linear scale is employed. This figure also illustrates the effect of changing the radial scaling of the impurity density itself; we have plotted alongside the mobility for the case described in equations (17) and (18) where regardless of the increased wire growth the linear density of the impurity layer remains constant. Those equations show that there is then an extra factor of R in the mobility, because the surface density becomes sparser with

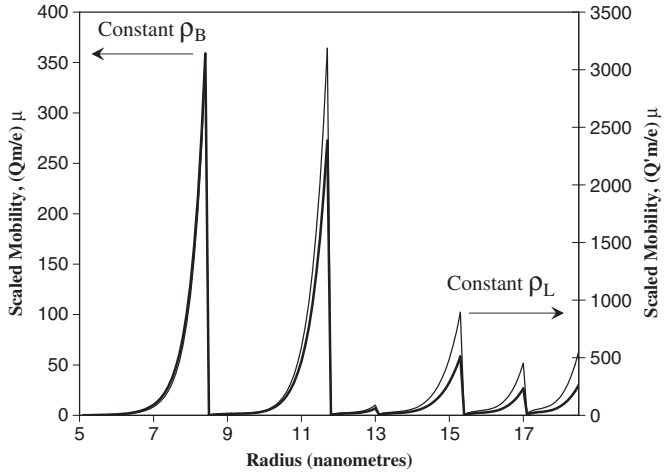

Figure 4. Plot of the scaled mobility versus the wire radius on a linear scale for constant bulk density of surface impurities (thick line, along the left axis) and for constant linear density (thin line, along the right axis). Note the scale factors are different for the two vertical axes, involving Q and Q' given by equations (16) and (18) respectively.

increased wire size; this causes the mobility to increase faster at larger radii as we see from the plot. Otherwise the two curves are quite similar, implying that the essential features are not affected significantly by the nature of the impurity distribution, because the strong exponential behaviour of the modified Bessel functions K_0 dominates the trend.

We have assumed a simple model which highlights general trends in the carrier mobility and related parameters as a semiconductor nanowire deviates from the strict size quantization limit towards bulk behaviour. Real semiconductor wires will not have a uniform cross-section, and are likely to have impurities in the wire interior as well as on the surface, so the behaviour we have seen will therefore likely be less sharp. Moreover, it is known that screening affects intra-band scattering more significantly [16, 23] than it does inter-band scattering. So a more accurate treatment of the dielectric function is likely to diminish the changes in the mobility as new channels become available. However, some recent works [24] indicate that a more rigorous treatment of impurity scattering could actually lead to higher values of the single channel mobility, in the regimes we consider, than those obtained using Fermi's Golden rule. This could actually contribute to accentuating the multichannel effects on the mobility by raising the maximum value it attains before undergoing a sharp drop due to a new scattering channel. The general trends we have established are sufficiently striking that those features would be relevant in experimentally observed behaviour of the mobility as the wire size is increased. In particular the effect of *inter*-channel scattering should be manifest in the degenerate limit.

Acknowledgments

The authors thank T Mayer, S Mohney, and J Redwing for helpful conversations. We acknowledge the support of NSF NIRT program grant DMR-0103068.

References

[1] Cui Y and Lieber C M 2001 *Science* **291** 851
[2] Cui Y, Zhong Z, Wang D, Wang W U and Lieber C M 2003 *Nano Lett.* **3** 149

[3] Ohlsson B J, Björk M T, Magnusson M H, Deppert K, Samuelson L and Wallenberg L R 2001 *Appl. Phys. Lett.* **79** 3335
[4] Hiruma K, Yazawa M, Haraguchi K, Ogawa K, Katsuyama T, Koguchi M and Kakibayashi H 1993 *J. Appl. Phys.* **74** 3162
[5] Wu Y and Yang P 2000 *Chem. Mater.* **12** 605
[6] Wang D, Wang Q, Javey A, Tu R, Dai H, Kim H, McIntyre P C, Krishnamohan T and Saraswat K C 2003 *Appl. Phys. Lett.* **83** 2432
[7] Duan X, Huang Y, Cui Y, Wang J and Lieber C M 2001 *Nature* **409** 6
[8] Bakkers E P A M, Van Dam J A, De Franceschi S, Kouwenhoven L P, Kaiser M, Verheijen M, Wondergem H and Van der Sluis P 2004 *Nat. Mater.* **3** 769
[9] Thelander C, Björk M T, Larsson M W, Hansen A E, Wallenberg L R and Samuelson L 2004 *Solid State Commun.* **131** 573
[10] Sakaki H 1981 *Japan. J. Appl. Phys.* **19** 148
[11] Lee J and Spector H N 1983 *J. Appl. Phys.* **54** 3921
[12] Lee J and Spector H N 1985 *J. Appl. Phys.* **57** 366
[13] Gold A and Ghazali A 1990 *Phys. Rev.* B **41** 7626
[14] Fishman G 1986 *Phys. Rev.* B **34** 2394
[15] DasSarma S and Xie X C 1987 *Phys. Rev.* B **35** 9875
[16] Weng Y and Leburton J P 1989 *J. Appl. Phys.* **65** 4983
[17] Manaselyan A K, Aghasyan M M and Kirakosyan A A 2002 *Physica* E **14** 366
[18] Sundaram V S and Mizel A 2004 *J. Phys.: Condens. Matter* **16** 4697
[19] Cui Y, Lauhon L J, Gudiksen M S and Wang J 2001 *Appl. Phys. Lett.* **78** 2214
[20] Holmes J D, Johnston K P, Doty R C and Korgel B A 2000 *Science* **287** 1471
[21] Gudisen M S and Lieber C M 2000 *J. Am. Chem. Soc.* **122** 8801
[22] Dingle R, Störmer H L, Gossard A C and Wiegmann W 1978 *Appl. Phys. Lett.* **33** 665
[23] Ferry D K and Goodnick S M 1997 *Transport in Nanostructures* (Cambridge: Cambridge University Press)
[24] Mŏsko M and Vagner P 1999 *Phys. Rev.* B **59** 10445